

Exploring the Structural Stability, Electronic and Thermal Attributes of synthetic 2D Materials and their Heterostructures

Ghulam Hussain^{a,*}, Mazia Asghar^b, Muhammad Waqas Iqbal^b, Hamid Ullah^{b,*}, Carmine Autieri^a

^aInternational Research Centre MagTop, Institute of Physics, Polish Academy of Sciences, Aleja Lotników 32/46, PL-02668 Warsaw, Poland

^bDepartment of Physics, Riphah International University, Campus Lahore, Pakistan

E-mail: ghussain@ifpan.edu.pl, hamid.ullah@riphah.edu.pk

ABSTRACT

Based on first-principles calculations, we have investigated the structural stability, electronic structures, and thermal properties of the monolayer XSi_2N_4 ($\text{X} = \text{Ti, Mo, W}$) and their lateral (LH) and vertical heterostructures (VH). We find that these heterostructures are energetically and dynamically stable due to high cohesive and binding energies, and no negative frequencies in the phonon spectra. The XSi_2N_4 ($\text{X} = \text{Ti, Mo, W}$) monolayers, the $\text{TiSi}_2\text{N}_4/\text{MoSi}_2\text{N}_4\text{-LH}$, $\text{MoSi}_2\text{N}_4/\text{WSi}_2\text{N}_4\text{-LH}$, and $\text{MoSi}_2\text{N}_4/\text{WSi}_2\text{N}_4\text{-VH}$ possess a semiconducting nature with an indirect band gap ranging from 0.30 to 2.60 eV. At room temperature, the C_v values are found to be between 100 and 416 $\text{JK}^{-1}\text{mol}^{-1}$ for the monolayers and their heterostructures, suggesting the better ability to retain heat with respect to transition metal dichalcogenides. Our study unveils the excellent attributes of XSi_2N_4 2D monolayers and their heterostructures, proposing them as potential candidates in nanoelectronics and thermoelectric applications.

1. Introduction

Due to the monolayer limit, the two-dimensional (2D) materials have distinct physical properties and thus are employable in a wide range of device applications [1-9]. Graphene, the first 2D material, has been widely studied since its discovery [3, 10]. It was expected to be a suitable layered structure for the new generation of nanoelectronic devices thanks to its high carrier mobility. However, graphene's zero band gap reminds us that it cannot be effective in many device applications [11-13]. On the other hand, transition metal dichalcogenides (TMDCs) are explored to exhibit tunable band gaps, but on account of practical applications, their relatively low carrier mobilities cannot be neglected [1, 14, 15]. For instance, MoS₂ possesses carrier mobility of approximately 200 cm²V⁻¹s⁻¹ for holes and 72 cm²V⁻¹s⁻¹ for electrons [14], which are much lower in magnitude than that of graphene and even much smaller than Si (480 cm²V⁻¹s⁻¹ for hole and 1350 cm²V⁻¹s⁻¹ for electron) [14, 16]. In recent years, from the fundamental and applicative point of view, we have assisted to tremendous efforts in the investigation of the topological and magnetic properties of the 2D materials and quasi-2D materials [17-25].

Recently, the discovery of novel 2D materials family, XA₂Z₄ (X=Transition metal, A=IV element, Z=V element) [26] has attracted broad consideration due to the outstanding properties they demonstrate. The first member of this assembly is the MoSi₂N₄ that was successfully produced via chemical vapor deposition (CVD) process with a large area of size 15 mm × 15 mm. This semiconducting material with a septuple-atomic-layer configuration (N-Si-N-Mo-N-Si-N) can be regarded as a MoN₂ layer sandwiched in two SiN layers, exhibiting an indirect band gap of almost 1.94 eV. The monolayer of MoSi₂N₄ depicts an elastic modulus that is roughly four times larger than MoS₂, and the carrier mobilities of holes and electrons are also four to six times that of a single layer of MoS₂. Moreover, a new family, namely XA₂Z₄ (X=Transition metal, A=IV element,

Z=V element) is anticipated by density functional theory (DFT) calculation. So far, several studies have been carried out describing the exceptional features of these materials [27-34].

Designing vertically stacked or laterally stitched two-dimensional heterostructures between 2D materials is an effective technique to unravel new features and extend their applications to electronics, detectors, electroluminescence, and photovoltaics [35-41]. Several experimental techniques such as physical vapor transport, CVD, plasma-assisted deposition, thermal decomposition, and vapor phase growth method have been utilized to synthesize the lateral heterostructures (LH) and vertical heterostructures (VH) [41-47]. Recently, the vertically stacked bilayer of MoSi_2N_4 have been studied using first-principles calculations, which reports the effect of strain on the electronic band gap, the bilayer MoSi_2N_4 showed a decrease in the band gap as the vertical strain was increased; and at around 22% strain, the bilayer revealed a semiconducting to metal transition [31]. Also, the band gap decreases as a function of the electric field for both the MoSi_2N_4 , and WSi_2N_4 bilayers, respectively [28]. Likewise, the vertical heterostructures of MoSi_2N_4 and MoGe_2N_4 have been reported, where the electronic properties and ferroelectricity are investigated [29, 30]. Nonetheless, the van der Waals heterostructures of this class are not explored thoroughly and demand a detailed study. In addition, the laterally stitched heterostructures of this novel family are not reported so far.

In this work using first-principle calculations, we carry out a detailed study of XSi_2N_4 (X= Ti, Mo, W) 2D monolayers and their lateral and vertical heterostructures such as $\text{TiSi}_2\text{N}_4/\text{MoSi}_2\text{N}_4$ and $\text{MoSi}_2\text{N}_4/\text{WSi}_2\text{N}_4$. All the compounds are investigated in their 2H crystal structure. The cohesive energies and the absence of imaginary phonon modes in the phonon dispersions exposed the structural stability of XSi_2N_4 systems and their lateral and vertical heterostructures. Since the electronic properties calculated by DFT are usually in poor agreement with the experiments,

principally the band gap, the Hybrid functional (HSE06) is applied to accurately approximate the electronic band structures. Both, the density of states and electronic band structures of XSi_2N_4 2D materials and their LHs and VHs indicated trivial indirect band gaps. In contrast, a semiconducting to metallic transition is observed in the vertical heterostructure of $\text{TiSi}_2\text{N}_4/\text{MoSi}_2\text{N}_4$. Compared to parent XSi_2N_4 materials, the lateral and vertical heterostructures show the highest free energy and heat capacity values. Our theoretical investigations could pave the path for designing novel nanoelectronic devices based on XSi_2N_4 and their hetero-systems.

2. Methodology

We performed first-principles calculation via the Vienna ab initio simulation package (VASP) [48, 49] using density functional theory (DFT). Both the Heyd-Scuseria-Ernzerhof (HSE06) and the generalized gradient approximation with PBE form [27] and [28] are adopted to calculate the electronic properties [50, 51]. For relaxation, an energy cutoff of 500 eV and a mesh of $15 \times 15 \times 1$ k-points were chosen. The periodic structures in the perpendicular direction of 2D material and heterostructure were separated with a vacuum layer of approximately 20 Å, which would avoid spurious interactions. Our calculations were converged by setting the convergence criteria to 0.01 eV/Å and energy 10^{-7} eV. To study the dynamical stability of XSi_2N_4 monolayers and that of LHs and VHs, PHONOPY code using a $4 \times 4 \times 1$ supercell was employed for calculating the phonon band structures [52]. Also, the thermal properties such as the heat capacity, free energy and entropy were explored using phonon calculations.

3. Results and discussions

Structural stability

The optimized structures for XSi_2N_4 ($\text{X}=\text{Ti, Mo, W}$) monolayers and their heterostructures are visualized in Fig. 1, where the (a), (b) and (c) panels depict the monolayer, lateral heterostructure (LH) and vertical heterostructures (VH), respectively. It can be seen that XSi_2N_4 ($\text{X}=\text{Ti, Mo, W}$) possesses a honeycomb structure consisting of Ti/Mo/W, Si and N atoms. The side view illustrates that this structure is stacked by seven atomic layers of N-Si-N-X-N-Si-N that exhibits a sandwich structure of MoN_2 layer by two SiN bilayers. We noticed the optimized lattice constants for XSi_2N_4 ($\text{X}=\text{Ti, Mo, W}$) monolayers to be $a = b = 2.932, 2.909$ and 2.915 \AA , respectively. These lattice constants are in perfect agreement with the calculated lattice parameters in the literature [26, 27, 53, 54]. Here, we consider the lateral AA- stitching for the LHs (Fig. 1b) and vertical AB-stacking for the VHs (Fig. 1c), the heterostructures obtained are $\text{TiSi}_2\text{N}_4/\text{MoSi}_2\text{N}_4\text{-LH}$, $\text{TiSi}_2\text{N}_4/\text{MoSi}_2\text{N}_4\text{-VH}$, $\text{MoSi}_2\text{N}_4/\text{WSi}_2\text{N}_4\text{-LH}$, and $\text{MoSi}_2\text{N}_4/\text{WSi}_2\text{N}_4\text{-VH}$. In the AA-stacking of VHs, all atoms i.e. the X, Si and N atoms of one monolayer of XSi_2N_4 are located exactly above the X, Si and N atoms of the other XSi_2N_4 layer. Whereas, in AB-stacking, all the atoms in the one XSi_2N_4 layer are staggered with respect to another XSi_2N_4 monolayer, as depicted in Fig. 1c. Based on total ground state energy calculations, the ground state is AB stacking [26, 28, 29].

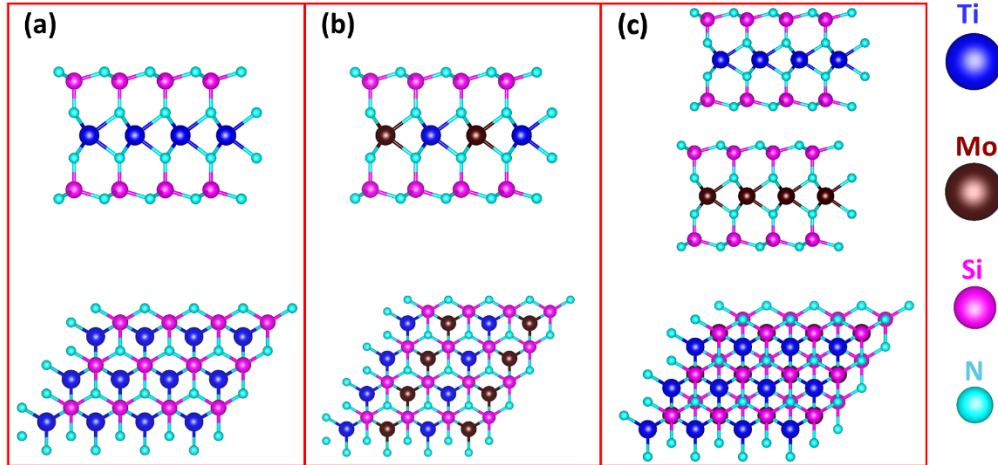


Figure 1 Side and top views of the atomic structures of (a) XSi_2N_4 monolayer, (b) lateral heterostructure (LH), and (c) vertical heterostructure (VH).

In order to check the stability of XSi_2N_4 monolayers and that of LHs and VHs, we used the total ground state energies to compute the cohesive energies. In addition, the phonon dispersions are calculated to determine their dynamical stability, which can enable the use of the studied systems in the device application. In the monolayer case of XSi_2N_4 , the cohesive energy is calculated by [55, 56];

$$E_c = \frac{1E_X + 2E_{\text{Si}} + 4E_{\text{N}} - E_{\text{XSi}_2\text{N}_4}}{1 + 2 + 4}$$

Here, E_X , E_{Si} , E_{N} and $E_{\text{XSi}_2\text{N}_4}$ are total ground state energies of isolated X, Si, N atoms and monolayer XSi_2N_4 , respectively. The cohesive energies for TiSi_2N_4 , MoSi_2N_4 and that of WSi_2N_4 are evaluated to be 5.562, 5.589 and 5.653 eV/atom, respectively. By comparing these values with that of graphene (7.46 eV/atom), MoS_2 (4.98 eV/atom) and phosphorene (3.30 eV/atom) [57-59], we noted that they are smaller than graphene but larger than MoS_2 , which indicate the better stability. For the heterostructures, the binding energies are estimated to determine the stability, it is given by [60];

$$E_b = E_{\text{heterostructure}} - E_{X^1\text{Si}_2\text{N}_4} - E_{X^2\text{Si}_2\text{N}_4}$$

Where $E_{\text{heterostructure}}$, denotes the total energy of the heterostructure while $E_{X^1\text{Si}_2\text{N}_4}$, $E_{X^2\text{Si}_2\text{N}_4}$ represent the ground state energies of the two monolayers involved in the formation of LH or VH. The binding energies for $\text{TiSi}_2\text{N}_4/\text{MoSi}_2\text{N}_4$ -LH, $\text{TiSi}_2\text{N}_4/\text{MoSi}_2\text{N}_4$ -VH, $\text{MoSi}_2\text{N}_4/\text{WSi}_2\text{N}_4$ -LH, and $\text{MoSi}_2\text{N}_4/\text{WSi}_2\text{N}_4$ -VH are -120.175 eV, -45.06 meV, -125.465 eV and -50.082 meV, respectively.

To examine the dynamical stability of XSi_2N_4 ($X=\text{Ti, Mo, W}$) monolayers and that of

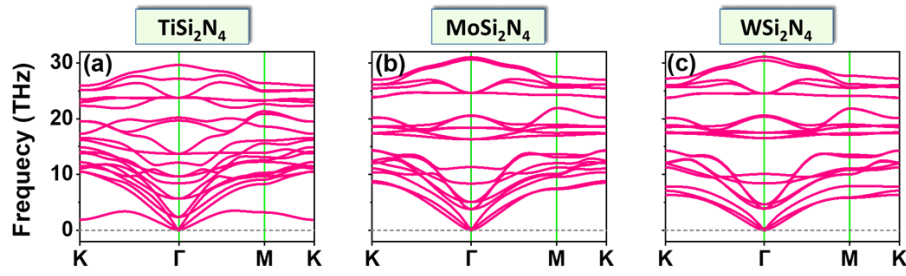


Figure 3 Phonon bandstructures for XSi_2N_4 ($X=\text{Ti, Mo, W}$) monolayers revealing no imaginary modes.

heterostructures, we carried out the phonon dispersion calculations as shown in Fig. 2 and 3. The

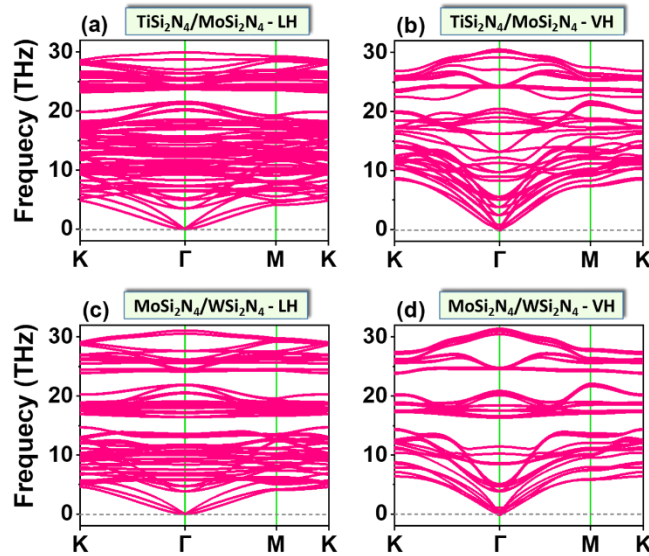


Figure 2 Calculated phonon dispersion curves of the lateral and vertical heterostructures for (a) $\text{TiSi}_2\text{N}_4/\text{MoSi}_2\text{N}_4$ -LH, (b) $\text{TiSi}_2\text{N}_4/\text{MoSi}_2\text{N}_4$ -VH, (c) $\text{MoSi}_2\text{N}_4/\text{WSi}_2\text{N}_4$ -LH and (d) $\text{MoSi}_2\text{N}_4/\text{WSi}_2\text{N}_4$ -VH.

finite difference method is employed to calculate the phonon spectra using the Phonopy code [52]

with VASP [61] as a calculator. From the phonon dispersion curves shown in Fig. 2, it is confirmed that all the three XSi_2N_4 ($\text{X}=\text{Ti}, \text{Mo}, \text{W}$) monolayers are dynamically stable due to the absence of imaginary modes. Similarly in Fig. 3, the calculated phonon band spectra along the Brillouin zone's high symmetry directions ($\text{K}-\Gamma-\text{M}-\text{K}$) for both the lateral and vertical heterostructures reveal no imaginary frequency at the Γ -point, indicating the dynamical stability of the corresponding systems. Interestingly, the soft acoustic mode of TiSi_2N_4 having a frequency of ~ 2 THz at the K-point (shown in Fig. 2a), becomes harder (increase in the frequency at same wave-vector) when TiSi_2N_4 is brought in combination with any XSi_2N_4 monolayer. This makes TiSi_2N_4 easier to synthesize in combination with other compounds. For $\text{TiSi}_2\text{N}_4/\text{MoSi}_2\text{N}_4\text{-LH}$ and $\text{TiSi}_2\text{N}_4/\text{MoSi}_2\text{N}_4\text{-VH}$, the hardening of this mode can be seen in Fig. 3a and 3b, respectively. The hardening of ~ 2 THz acoustic mode occurring at the K-point can be ascribed to the enhanced coupling at this wave-vector [62, 63].

Electronic properties

To understand the contribution of different orbitals from various elements that characterize our systems' electronic attributes, the total density of states (TDOS) and partial density of states (PDOS) are computed. Figure 4 illustrates the TDOS and PDOS for the respective XSi_2N_4 monolayers. For the monolayer TiSi_2N_4 , the valence band maximum (VBM) is mainly dominated by N atoms ' p ' orbitals with slight contribution from Ti- d orbitals, while the conduction band minima (CBM) is principally originated by the Ti- d orbital, as illustrated in Fig. 4a. In the case of MoSi_2N_4 , and WSi_2N_4 , however, both the VBMs and CBMs maximally arise due to the Mo-/W- d orbitals, which are located in the middle of each monolayer structure (Fig. 4b, c).

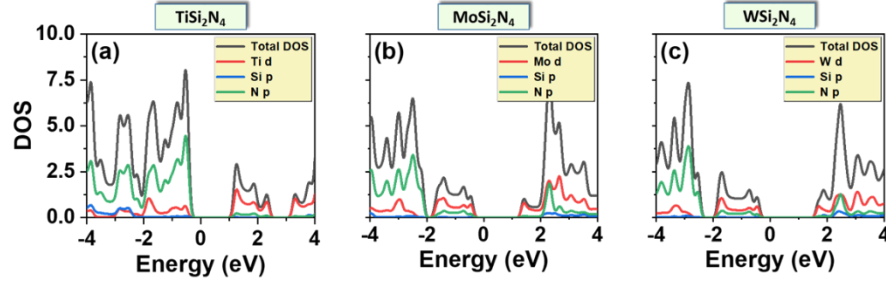


Figure 4 Calculated TDOS and PDOS of (a) TiSi_2N_4 , (b) MoSi_2N_4 and (c) WSi_2N_4 monolayers. The Fermi-level is set to zero energy.

In Fig. 5, we investigate the TDOS and PDOS for the heterostructures including $\text{TiSi}_2\text{N}_4/\text{MoSi}_2\text{N}_4$ -LH, $\text{TiSi}_2\text{N}_4/\text{MoSi}_2\text{N}_4$ -VH, $\text{MoSi}_2\text{N}_4/\text{WSi}_2\text{N}_4$ -LH, and $\text{MoSi}_2\text{N}_4/\text{WSi}_2\text{N}_4$ -VH. Figure 5(a), exhibits that the band gap decreases to a very small value of 0.137 eV for $\text{TiSi}_2\text{N}_4/\text{MoSi}_2\text{N}_4$ -LH whereby the VBM is dominated by Mo-*d* orbitals with little contributions from N-*p* and Ti-*d* orbitals, whereas the CBM is maximally originated by N-*p* and Ti-*d* orbitals. Interestingly, the $\text{TiSi}_2\text{N}_4/\text{MoSi}_2\text{N}_4$ -VH shows metallicity thereby appearing a considerable DOS at the Fermi level as shown in Fig. 5b. This metallic behavior of the VH is mainly contributed by Ti '*d*' orbitals and partly by Mo '*d*' and N '*p*' orbitals. Differently from these two heterostructures of $\text{TiSi}_2\text{N}_4/\text{MoSi}_2\text{N}_4$, the lateral and vertical heterostructures of $\text{MoSi}_2\text{N}_4/\text{WSi}_2\text{N}_4$ manifest large band gaps as shown in Fig. 5c and 5d. For $\text{MoSi}_2\text{N}_4/\text{WSi}_2\text{N}_4$ -LH, both the VBM and CBM are dominated mainly by the '*d*' orbitals of Mo and W. Similarly, the VBM of $\text{MoSi}_2\text{N}_4/\text{WSi}_2\text{N}_4$ -VH maximally arise due to the '*d*' orbitals of Mo and W, while the CBM is contributed by Mo '*d*' orbitals only. In conclusion, all the structures including XSi_2N_4 materials and their heterostructures reveal trivial insulating behavior, except the VH of $\text{TiSi}_2\text{N}_4/\text{MoSi}_2\text{N}_4$, which is metallic.

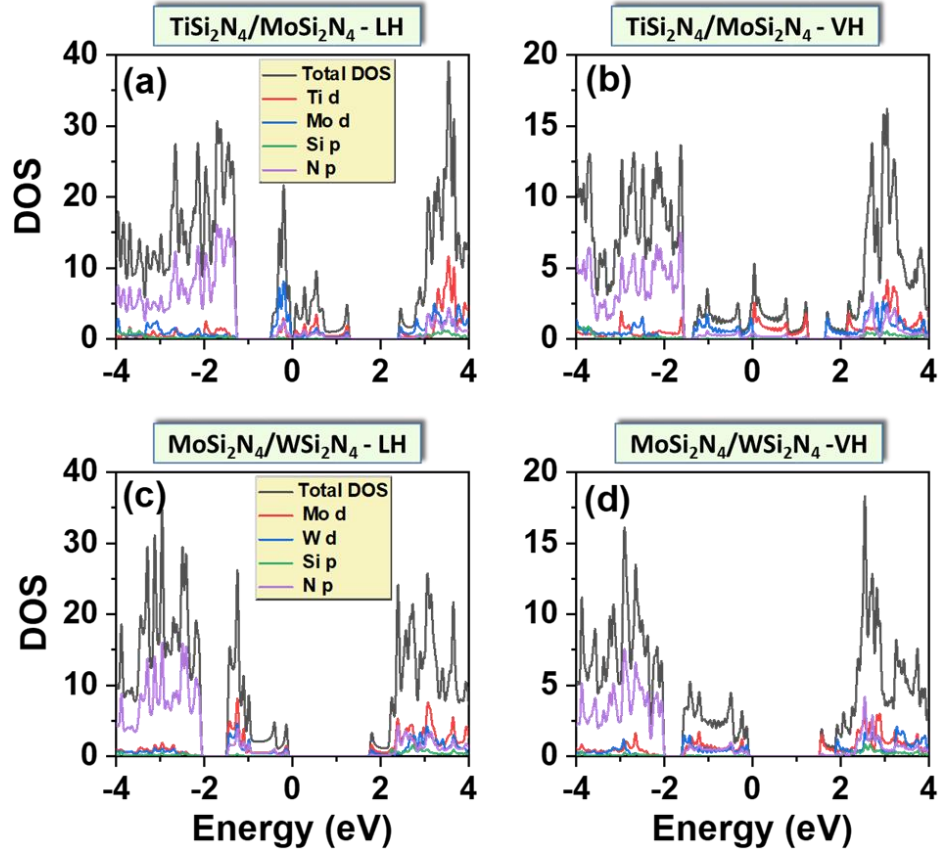


Figure 5 Calculated TDOS and PDOS of (a) $\text{TiSi}_2\text{N}_4/\text{MoSi}_2\text{N}_4$ -LH, (b) $\text{TiSi}_2\text{N}_4/\text{MoSi}_2\text{N}_4$ -VH, (c) $\text{MoSi}_2\text{N}_4/\text{WSi}_2\text{N}_4$ -LH, and (d) $\text{MoSi}_2\text{N}_4/\text{WSi}_2\text{N}_4$ -VH. The Fermi-level is set to zero energy.

The electronic band structures were calculated to further investigate the electronic properties of XSi_2N_4 ($\text{X}=\text{Ti}, \text{Mo}, \text{W}$) monolayers and their heterostructures. Since the electronic band gaps calculated by DFT are usually in poor agreement with the experiments and mostly underestimated [64-66], therefore, the Hybrid functional (HSE06) [50] is applied to approximate the electronic band structures. Figure 6 demonstrates the band structures of XSi_2N_4 materials and heterostructures computed through both PBE and HSE06 potentials. The XSi_2N_4 ($\text{X}=\text{Ti}, \text{Mo}, \text{W}$) monolayers possess an indirect band gap of 2.61 eV, 2.35 eV, and 2.69 eV for TiSi_2N_4 , MoSi_2N_4 , and WSi_2N_4 , respectively, as shown in Fig. 6a, b, c. For the $\text{TiSi}_2\text{N}_4/\text{MoSi}_2\text{N}_4$ -LH, the maximum of the valence band (VBM) appears at the M-point, while the minimum of the conduction band

(CBM) occurs at the Γ -point (Fig. 6d). On the other hand, in the cases of $\text{MoSi}_2\text{N}_4/\text{WSi}_2\text{N}_4\text{-LH}$ and $\text{MoSi}_2\text{N}_4/\text{WSi}_2\text{N}_4\text{-VH}$, the VBM emerges at Γ -point, whereas the CBM occurs at the K-point, as can be seen in Fig. 6e, f, suggesting that the indirect band gap nature still prevails. The values of the indirect band gaps are determined to be ~ 0.30 , 2.34, and 2.15 eV for the $\text{TiSi}_2\text{N}_4/\text{MoSi}_2\text{N}_4\text{-LH}$, $\text{MoSi}_2\text{N}_4/\text{WSi}_2\text{N}_4\text{-LH}$, and $\text{MoSi}_2\text{N}_4/\text{WSi}_2\text{N}_4\text{-VH}$, respectively, which could make them promising for the application in solar cells and optoelectronic devices [67-70]. The calculated band gap values are tabulated in Table 1, which are in agreement with the available literature [27, 31, 33]. A slight difference in band gaps may arise due to the difference in lattice parameters.

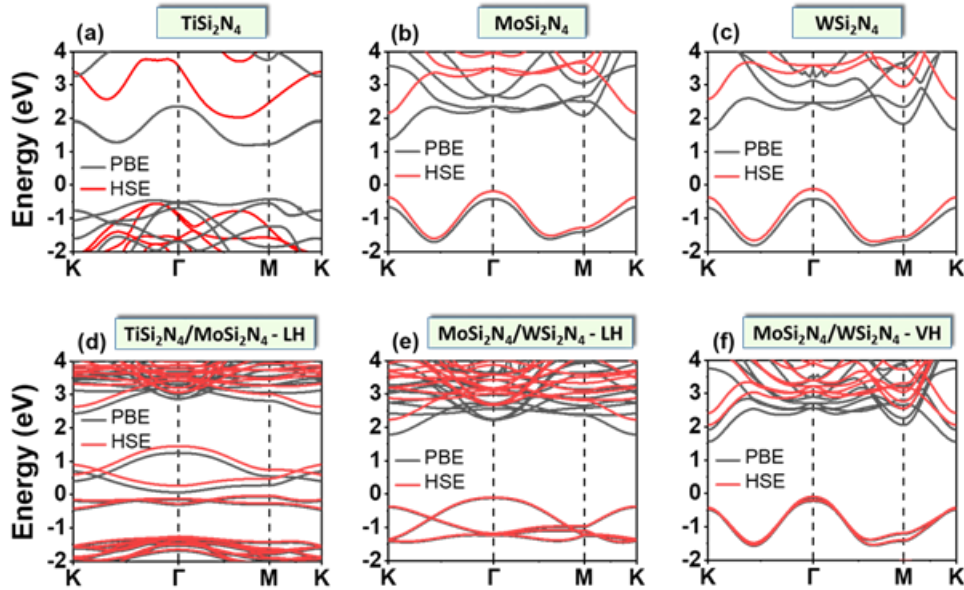


Figure 6 Electronic band structures calculated through PBE (black color) and HSE06 (red color) for (a) TiSi_2N_4 , (b) MoSi_2N_4 , (c) WSi_2N_4 , (d) $\text{TiSi}_2\text{N}_4/\text{MoSi}_2\text{N}_4\text{-LH}$, (e) $\text{MoSi}_2\text{N}_4/\text{WSi}_2\text{N}_4\text{-LH}$ and (f) $\text{MoSi}_2\text{N}_4/\text{WSi}_2\text{N}_4\text{-VH}$.

Table 1 Calculated electronic band gaps of XSi_2N_4 materials and their lateral and vertical heterostructures using PBE and HSE06.

Material	PBE Band gap (eV)	HSE Band gap (eV)
TiSi_2N_4	1.63	2.40
MoSi_2N_4	1.74	2.35
WSi_2N_4	2.12	2.60
$\text{TiSi}_2\text{N}_4/\text{MoSi}_2\text{N}_4 - \text{LH}$	0.14	0.30
$\text{MoSi}_2\text{N}_4/\text{WSi}_2\text{N}_4 - \text{LH}$	1.90	2.34
$\text{MoSi}_2\text{N}_4/\text{WSi}_2\text{N}_4 - \text{VH}$	1.70	2.15

Thermal properties

Based on the stable phonon dispersions of XSi_2N_4 ($\text{X}=\text{Ti}, \text{Mo}, \text{W}$) monolayers and their heterostructures, the thermal characteristics including entropy (S), Helmholtz free energy (F), and heat capacity C_v are calculated as shown in Figure 7. The entropy of all the systems rises steadily with the temperature, consistently with the fact that increasing the temperature gives rise to several microstates in the system W , which results in an increase in the entropy logarithmically according to the Boltzmann's entropy formula ($S = k_B \log W$, where k_B is the Boltzmann constant). On the other hand, the Helmholtz free energy, F , is observed to decline with temperature, as shown in Fig. 7b and 7e, which agrees with $F(T) = U(T) - TS(T)$; $U(T)$ is the lattice internal energy. Furthermore, we investigate the heat capacity C_v of XSi_2N_4 ($\text{X}=\text{Ti}, \text{Mo}, \text{W}$) monolayers and their heterostructures as a function of temperature as illustrated in Fig. 7c and 7f. Comparable heat capacities of TiSi_2N_4 , MoSi_2N_4 and WSi_2N_4 are observed as reported in Fig. 7c and 7f.

Intriguingly, the heat capacity increases for the VHS and further enhances for the LHS. At room temperature, the C_v values are estimated to be 106.1, 100.5, 100.8, 206.5, 415.6, 201.3 and 402.3 $\text{JK}^{-1}\text{mol}^{-1}$ for TiSi_2N_4 , MoSi_2N_4 , WSi_2N_4 , $\text{TiSi}_2\text{N}_4/\text{MoSi}_2\text{N}_4\text{-VH}$, $\text{TiSi}_2\text{N}_4/\text{MoSi}_2\text{N}_4\text{-LH}$, $\text{MoSi}_2\text{N}_4/\text{WSi}_2\text{N}_4\text{-VH}$ and $\text{MoSi}_2\text{N}_4/\text{WSi}_2\text{N}_4\text{-LH}$, respectively. Our estimated values of C_v are relatively higher than PbSe and PbTe [71, 72] (which are thought to be excellent thermoelectric materials), suggesting the better ability of XSi_2N_4 ($\text{X}=\text{Ti, Mo, W}$) monolayers and their heterostructures to retain heat. The heat capacity of XSi_2N_4 ($\text{X}=\text{Ti, Mo, W}$) monolayers takes the lead to approach the Dulong-petit asymptotic value (i.e. $C_v = 3NR$, where N is the number of atoms and R is the universal gas constant) at around $T \sim 560$ K. Whereas, the VHS of $\text{TiSi}_2\text{N}_4/\text{MoSi}_2\text{N}_4$, and $\text{MoSi}_2\text{N}_4/\text{WSi}_2\text{N}_4$ approach this asymptote at a relatively higher temperature, near $T \sim 650$ K, and LHS of $\text{TiSi}_2\text{N}_4/\text{MoSi}_2\text{N}_4$, and $\text{MoSi}_2\text{N}_4/\text{WSi}_2\text{N}_4$ required a higher temperature of around $T \sim 750$ K and $T \sim 850$ K to approach this value. From this investigation, we found that C_v is consistent with the entropy we computed here since the variation of entropy corresponds to the integral of (C_v/T) over a given temperature range.

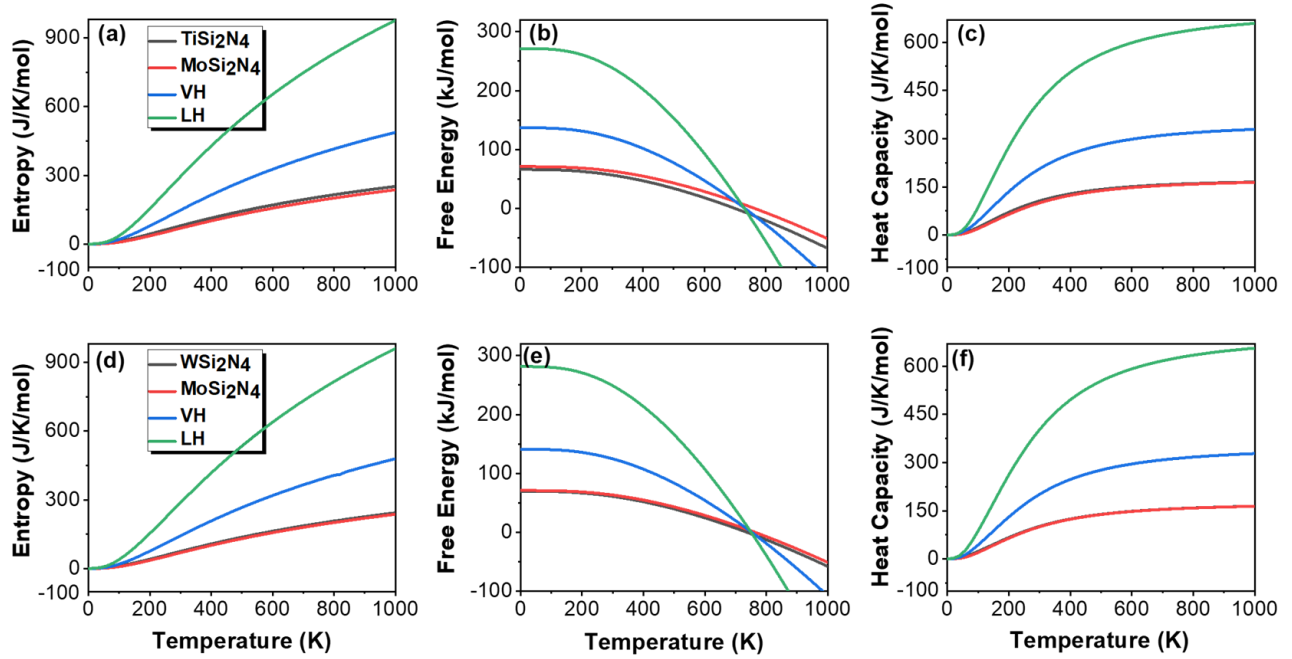


Figure 7 Thermal properties such as entropy, free energy and heat capacity. The top panels (a), (b) and (c) represent TiSi_2N_4 , MoSi_2N_4 and their lateral and vertical heterostructures, while the lower panel characterizes MoSi_2N_4 , WSi_2N_4 , and their lateral and vertical heterostructures.

4. Conclusions

The structural stability, electronic properties and thermal characteristics of XSi_2N_4 ($\text{X} = \text{Ti}, \text{Mo}, \text{W}$) monolayers and their lateral and vertical heterostructures are explored using density functional theory. We noticed that interfacing two different 2D structures either laterally or vertically, significantly tunes the physical properties of the parent 2D monolayers that may have technological impact in many potential applications. The structural stability of these systems was confirmed by the cohesive energies which are based on the total ground state energies and the phonon dispersions revealing the dynamical stability. Apart from their stability, our results illustrated that the lateral and vertical heterostructures present outstanding electronic and thermal features. All the three monolayers i.e. TiSi_2N_4 , MoSi_2N_4 , and WSi_2N_4 revealed indirect band gaps. Remarkably, a semiconducting to metallic transition is observed in the VH of $\text{TiSi}_2\text{N}_4/\text{MoSi}_2\text{N}_4$,

while the LH of $\text{TiSi}_2\text{N}_4/\text{MoSi}_2\text{N}_4$ manifested a small band gap. Both the lateral and vertical heterostructures of $\text{MoSi}_2\text{N}_4/\text{WSi}_2\text{N}_4$ revealed semiconducting nature with modifications in their band gaps with respect to the parent monolayers. Compared to the transition metal dichalcogenides, the monolayers XSi_2N_4 and their heterostructures bear the highest values for the free energy and heat capacity. The study suggests that both the XSi_2N_4 2D monolayers and their heterostructures could be promising in the next-generation optoelectronics and nanoelectronics.

Acknowledgments

This work is supported by the Foundation for Polish Science through the international research agendas program co-financed by the European Union within the smart growth operational program. We acknowledge the access to the computing facilities of the Interdisciplinary Center of Modeling at the University of Warsaw, Grants No. GB84-0 and No. GB84-7. The authors extend their appreciation to Riphah International University for funding this work under project number R-ORIC-21/FEAS-10.

References

- [1] Q.H. Wang, K. Kalantar-Zadeh, A. Kis, J.N. Coleman, M.S. Strano, Electronics and optoelectronics of two-dimensional transition metal dichalcogenides, *Nature nanotechnology*, 7 (2012) 699-712.
- [2] W. Hou, H. Mi, R. Peng, S. Peng, W. Zeng, Q. Zhou, First-principle insight into Ga-doped MoS₂ for sensing SO₂, SOF₂ and SO₂F₂, *Nanomaterials*, 11 (2021) 314.
- [3] K.S. Novoselov, A.K. Geim, S.V. Morozov, D.-e. Jiang, Y. Zhang, S.V. Dubonos, I.V. Grigorieva, A.A. Firsov, Electric field effect in atomically thin carbon films, *science*, 306 (2004) 666-669.
- [4] T. Yu, Z. Zhao, Y. Sun, A. Bergara, J. Lin, S. Zhang, H. Xu, L. Zhang, G. Yang, Y. Liu, Two-dimensional PC6 with direct band gap and anisotropic carrier mobility, *Journal of the American Chemical Society*, 141 (2019) 1599-1605.
- [5] L. Ci, L. Song, C. Jin, D. Jariwala, D. Wu, Y. Li, A. Srivastava, Z. Wang, K. Storr, L. Balicas, Atomic layers of hybridized boron nitride and graphene domains, *Nature materials*, 9 (2010) 430-435.
- [6] Y. Zhang, Y.-W. Tan, H.L. Stormer, P. Kim, Experimental observation of the quantum Hall effect and Berry's phase in graphene, *nature*, 438 (2005) 201-204.
- [7] Y. Lin, T.V. Williams, J.W. Connell, Soluble, exfoliated hexagonal boron nitride nanosheets, *The Journal of Physical Chemistry Letters*, 1 (2010) 277-283.
- [8] W. Wu, P. Lu, Z. Zhang, W. Guo, Electronic and magnetic properties and structural stability of BeO sheet and nanoribbons, *ACS applied materials & interfaces*, 3 (2011) 4787-4795.
- [9] Z. Zhang, X. Liu, B.I. Yakobson, W. Guo, Two-dimensional tetragonal TiC monolayer sheet and nanoribbons, *Journal of the American Chemical Society*, 134 (2012) 19326-19329.

- [10] A.K. Geim, K.S. Novoselov, The rise of graphene, in: Nanoscience and technology: a collection of reviews from nature journals, World Scientific, 2010, pp. 11-19.
- [11] K.S. Novoselov, A.K. Geim, S.V. Morozov, D. Jiang, M.I. Katsnelson, I. Grigorieva, S. Dubonos, Firsov, AA, Two-dimensional gas of massless Dirac fermions in graphene, nature, 438 (2005) 197-200.
- [12] A. Lherbier, A.R. Botello-Méndez, J.-C. Charlier, Electronic and transport properties of unbalanced sublattice N-doping in graphene, Nano letters, 13 (2013) 1446-1450.
- [13] J. Chen, J. Xi, D. Wang, Z. Shuai, Carrier mobility in graphyne should be even larger than that in graphene: a theoretical prediction, The journal of physical chemistry letters, 4 (2013) 1443-1448.
- [14] Y. Cai, G. Zhang, Y.-W. Zhang, Polarity-reversed robust carrier mobility in monolayer MoS₂ nanoribbons, Journal of the American Chemical Society, 136 (2014) 6269-6275.
- [15] K.F. Mak, C. Lee, J. Hone, J. Shan, T.F. Heinz, Atomically thin MoS₂: a new direct-gap semiconductor, Physical review letters, 105 (2010) 136805.
- [16] G. Ludwig, R. Watters, Drift and conductivity mobility in silicon, Physical Review, 101 (1956) 1699.
- [17] Y. Ren, Z. Qiao, Q. Niu, Topological phases in two-dimensional materials: a review, Reports on Progress in Physics, 79 (2016) 066501.
- [18] H. Huang, Y. Xu, J. Wang, W. Duan, Emerging topological states in quasi-two-dimensional materials, Wiley Interdisciplinary Reviews: Computational Molecular Science, 7 (2017) e1296.
- [19] L. Kou, Y. Ma, Z. Sun, T. Heine, C. Chen, Two-dimensional topological insulators: Progress and prospects, The journal of physical chemistry letters, 8 (2017) 1905-1919.

- [20] X. Qian, J. Liu, L. Fu, J. Li, Quantum spin Hall effect in two-dimensional transition metal dichalcogenides, *Science*, 346 (2014) 1344-1347.
- [21] S. Kumari, D.K. Pradhan, N.R. Pradhan, P.D. Rack, Recent developments on 2D magnetic materials: challenges and opportunities, *Emergent Materials*, (2021) 1-20.
- [22] T. Van Thiel, W. Brzezicki, C. Autieri, J. Hortensius, D. Afanasiev, N. Gauquelin, D. Jannis, N. Janssen, D. Groenendijk, J. Fatermans, Coupling charge and topological reconstructions at polar oxide interfaces, *Physical Review Letters*, 127 (2021) 127202.
- [23] A. Lau, T. Hyart, C. Autieri, A. Chen, D.I. Pikulin, Designing Three-Dimensional Flat Bands in Nodal-Line Semimetals, *Physical Review X*, 11 (2021) 031017.
- [24] W. Lei, W. Wang, X. Ming, S. Zhang, G. Tang, X. Zheng, H. Li, C. Autieri, Structural transition, metallization, and superconductivity in quasi-two-dimensional layered PdS_2 under compression, *Physical Review B*, 101 (2020) 205149.
- [25] W. Wang, B. Wang, Z. Gao, G. Tang, W. Lei, X. Zheng, H. Li, X. Ming, C. Autieri, Charge density wave instability and pressure-induced superconductivity in bulk 1 T-NbS₂, *Physical Review B*, 102 (2020) 155115.
- [26] Y.-L. Hong, Z. Liu, L. Wang, T. Zhou, W. Ma, C. Xu, S. Feng, L. Chen, M.-L. Chen, D.-M. Sun, Chemical vapor deposition of layered two-dimensional MoSi_2N_4 materials, *Science*, 369 (2020) 670-674.
- [27] X. Lv, Y. Xu, B. Mao, G. Liu, G. Zhao, J. Yang, Strain modulation of electronic and optical properties of monolayer MoSi_2N_4 , *Physica E: Low-dimensional Systems and Nanostructures*, 135 (2022) 114964.
- [28] Q. Wu, L. Cao, Y.S. Ang, L.K. Ang, Semiconductor-to-metal transition in bilayer MoSi_2N_4 and WSi_2N_4 with strain and electric field, *Applied Physics Letters*, 118 (2021) 113102.

- [29] T. Zhong, Y. Ren, Z. Zhang, J. Gao, M. Wu, Sliding ferroelectricity in two-dimensional MoA_2N_4 (A= Si or Ge) bilayers: high polarizations and Moiré potentials, *Journal of Materials Chemistry A*, (2021).
- [30] D. Pham, Electronic properties of a two-dimensional van der Waals $\text{MoGe}_2\text{N}_4/\text{MoSi}_2\text{N}_4$ heterobilayer: effect of the insertion of a graphene layer and interlayer coupling, *RSC Advances*, 11 (2021) 28659-28666.
- [31] H. Zhong, W. Xiong, P. Lv, J. Yu, S. Yuan, Strain-induced semiconductor to metal transition in MA_2Z_4 bilayers (M= Ti, Cr, Mo; A= Si; Z= N, P), *Physical Review B*, 103 (2021) 085124.
- [32] A. Bafekry, M. Faraji, M.M. Fadlallah, A.B. Khatibani, A. abdolahzadeh Ziabari, M. Ghergherehchi, S. Nedaei, S.F. Shayesteh, D. Gogova, Tunable electronic and magnetic properties of MoSi_2N_4 monolayer via vacancy defects, atomic adsorption and atomic doping, *Applied Surface Science*, 559 (2021) 149862.
- [33] A. Bafekry, M. Faraji, D. Hoat, M. Shahrokhi, M. Fadlallah, F. Shojaei, S. Feghhi, M. Ghergherehchi, D. Gogova, MoSi_2N_4 single-layer: a novel two-dimensional material with outstanding mechanical, thermal, electronic and optical properties, *Journal of Physics D: Applied Physics*, 54 (2021) 155303.
- [34] R. Islam, B. Ghosh, C. Autieri, S. Chowdhury, A. Bansil, A. Agarwal, B. Singh, Tunable spin polarization and electronic structure of bottom-up synthesized MoSi_2N_4 materials, *Phys. Rev. B* 104, L201112, (2021).
- [35] L. Britnell, R.M. Ribeiro, A. Eckmann, R. Jalil, B.D. Belle, A. Mishchenko, Y.-J. Kim, R.V. Gorbachev, T. Georgiou, S.V. Morozov, Strong light-matter interactions in heterostructures of atomically thin films, *Science*, 340 (2013) 1311-1314.

- [36] W.J. Yu, Z. Li, H. Zhou, Y. Chen, Y. Wang, Y. Huang, X. Duan, Vertically stacked multi-heterostructures of layered materials for logic transistors and complementary inverters, *Nature materials*, 12 (2013) 246-252.
- [37] R. Moriya, T. Yamaguchi, Y. Inoue, S. Morikawa, Y. Sata, S. Masubuchi, T. Machida, Large current modulation in exfoliated-graphene/MoS₂/metal vertical heterostructures, *Applied Physics Letters*, 105 (2014) 083119.
- [38] W.J. Yu, Y. Liu, H. Zhou, A. Yin, Z. Li, Y. Huang, X. Duan, Highly efficient gate-tunable photocurrent generation in vertical heterostructures of layered materials, *Nature nanotechnology*, 8 (2013) 952-958.
- [39] P.T.K. Loan, W. Zhang, C.T. Lin, K.H. Wei, L.J. Li, C.H. Chen, Graphene/MoS₂ heterostructures for ultrasensitive detection of DNA hybridisation, *Advanced Materials*, 26 (2014) 4838-4844.
- [40] F. Withers, O. Del Pozo-Zamudio, A. Mishchenko, A. Rooney, A. Gholinia, K. Watanabe, T. Taniguchi, S.J. Haigh, A. Geim, A. Tartakovskii, Light-emitting diodes by band-structure engineering in van der Waals heterostructures, *Nature materials*, 14 (2015) 301-306.
- [41] M.-Y. Li, C.-H. Chen, Y. Shi, L.-J. Li, Heterostructures based on two-dimensional layered materials and their potential applications, *Materials Today*, 19 (2016) 322-335.
- [42] M.P. Levendorf, C.-J. Kim, L. Brown, P.Y. Huang, R.W. Havener, D.A. Muller, J. Park, Graphene and boron nitride lateral heterostructures for atomically thin circuitry, *Nature*, 488 (2012) 627-632.
- [43] X. Duan, C. Wang, J.C. Shaw, R. Cheng, Y. Chen, H. Li, X. Wu, Y. Tang, Q. Zhang, A. Pan, Lateral epitaxial growth of two-dimensional layered semiconductor heterojunctions, *Nature nanotechnology*, 9 (2014) 1024-1030.

- [44] W. Yang, G. Chen, Z. Shi, C.-C. Liu, L. Zhang, G. Xie, M. Cheng, D. Wang, R. Yang, D. Shi, Epitaxial growth of single-domain graphene on hexagonal boron nitride, *Nature materials*, 12 (2013) 792-797.
- [45] Y. Shi, W. Zhou, A.-Y. Lu, W. Fang, Y.-H. Lee, A.L. Hsu, S.M. Kim, K.K. Kim, H.Y. Yang, L.-J. Li, van der Waals epitaxy of MoS₂ layers using graphene as growth templates, *Nano letters*, 12 (2012) 2784-2791.
- [46] Y.-C. Lin, N. Lu, N. Perea-Lopez, J. Li, Z. Lin, X. Peng, C.H. Lee, C. Sun, L. Calderin, P.N. Browning, Direct synthesis of van der Waals solids, *Acs Nano*, 8 (2014) 3715-3723.
- [47] Y. Gong, J. Lin, X. Wang, G. Shi, S. Lei, Z. Lin, X. Zou, G. Ye, R. Vajtai, B.I. Yakobson, Vertical and in-plane heterostructures from WS₂/MoS₂ monolayers, *Nature materials*, 13 (2014) 1135-1142.
- [48] P.E. Blöchl, Projector augmented-wave method, *Physical review B*, 50 (1994) 17953.
- [49] G. Kresse, J. Furthmüller, Efficient iterative schemes for ab initio total-energy calculations using a plane-wave basis set, *Physical review B*, 54 (1996) 11169.
- [50] J. Heyd, G.E. Scuseria, M. Ernzerhof, Hybrid functionals based on a screened Coulomb potential, *The Journal of chemical physics*, 118 (2003) 8207-8215.
- [51] J.P. Perdew, K. Burke, M. Ernzerhof, Generalized gradient approximation made simple, *Physical review letters*, 77 (1996) 3865.
- [52] A. Togo, I. Tanaka, First principles phonon calculations in materials science, *Scripta Materialia*, 108 (2015) 1-5.
- [54] L. Tan, C. Nie, Z. Ao, H. Sun, T. An, S. Wang, Novel two-dimensional crystalline carbon nitrides beyond gC₃N₄: structure and applications, *Journal of Materials Chemistry A*, 9 (2021) 17-33.

- [55] M. Marques, E. Gross, A primer in density functional theory, Lecture Notes in Physics, 620 (2003) 144-184.
- [56] R. LeSar, Introduction to computational materials science: fundamentals to applications, Cambridge University Press, 2013.
- [57] J. Guan, Z. Zhu, D. Tománek, Phase coexistence and metal-insulator transition in few-layer phosphorene: a computational study, Physical review letters, 113 (2014) 046804.
- [58] P.-J. Chen, H.-T. Jeng, High applicability of two-dimensional phosphorous in Kagome lattice predicted from first-principles calculations, Scientific reports, 6 (2016) 1-8.
- [59] S. Ahmad, S. Mukherjee, A comparative study of electronic properties of bulk MoS₂ and its monolayer using DFT technique: application of mechanical strain on MoS₂ monolayer, (2014).
- [60] F.C. Hagemeister, C.J. Gruenloh, T.S. Zwier, Density functional theory calculations of the structures, binding energies, and infrared spectra of methanol clusters, The Journal of Physical Chemistry A, 102 (1998) 82-94.
- [61] J. Paier, M. Marsman, G. Kresse, Dielectric properties and excitons for extended systems from hybrid functionals, Physical Review B, 78 (2008) 121201.
- [62] J.M. Wesselinowa, Hardening and softening of soft phonon modes in ferroelectric thin films, Physical Review B, 75 (2007) 045411.
- [63] D. Phelan, M. Krogstad, N. Schreiber, R. Osborn, A. Said, H. Zheng, S. Rosenkranz, Acoustic phonon dispersion and diffuse scattering across the valence transition of (Pr_{0.85}Y_{0.15})_{0.7}Ca_{0.3}CoO₃– δ , Physical Review B, 100 (2019) 054101.
- [64] J. Heyd, J.E. Peralta, G.E. Scuseria, R.L. Martin, Energy band gaps and lattice parameters evaluated with the Heyd-Scuseria-Ernzerhof screened hybrid functional, The Journal of chemical physics, 123 (2005) 174101.

- [65] M. Alam, H.S. Waheed, H. Ullah, M.W. Iqbal, Y.-H. Shin, M.J.I. Khan, H. Elsaedy, R. Neffati, Optoelectronics properties of Janus SnSSe monolayer for solar cells applications, *Physica B: Condensed Matter*, 625 (2022) 413487.
- [66] M.W. Iqbal, M. Asghar, N. Noor, H. Ullah, T. Zahid, S. Aftab, A. Mahmood, Analysis of ternary AlGaX₂ (X= As, Sb) compounds for opto-electronic and renewable energy devices using density functional theory, *Physica Scripta*, 96 (2021) 125706.
- [67] L.A. Burton, Y. Kumagai, A. Walsh, F. Oba, DFT investigation into the underperformance of sulfide materials in photovoltaic applications, *Journal of Materials Chemistry A*, 5 (2017) 9132-9140.
- [68] P. Cheng, T. Wu, J. Zhang, Y. Li, J. Liu, L. Jiang, X. Mao, R.-F. Lu, W.-Q. Deng, K. Han, (C₆H₅C₂H₄NH₃)₂GeI₄: a layered two-dimensional perovskite with potential for photovoltaic applications, *The journal of physical chemistry letters*, 8 (2017) 4402-4406.
- [69] M. Afsari, A. Boochani, F. Shirdel, Electronic and optical properties of two propounded compound in photovoltaic applications, CsPbI₃ and CH₃NH₃PbI₃: By DFT, *Optik*, 199 (2019) 163360.
- [70] S. Roy, P. Bermel, Electronic and optical properties of ultra-thin 2D tungsten disulfide for photovoltaic applications, *Solar Energy Materials and Solar Cells*, 174 (2018) 370-379.
- [71] A. Pashinkin, M. Mikhailova, A. Malkova, V. Fedorov, Heat capacity and thermodynamic properties of lead selenide and lead telluride, *Inorganic Materials*, 45 (2009) 1226-1229.
- [72] D. Parkinson, J. Quarrington, The molar heats of lead sulphide, selenide and telluride in the temperature range 20 K to 260 K, *Proceedings of the Physical Society. Section A*, 67 (1954) 569.